Complementary Use of Active Infrared Thermography and Optical Coherent Tomography in Non-destructive Testing Inspection of Ancient Marquetries

Francisco J. Madruga[1] · Stefano Sfarra[2,3] · Eusebio Real[1] · Gianfranco Gargiulo[4] · Olga M. Conde[1] · Jose M. López-Higuera[1]

Abstract

Imaging-based inspection techniques have practical advantages in the study and/or rehabilitation of artworks. They provide in some cases internal information on the status of the sample to be inspected. On the one hand, techniques based on active infrared thermography (IRT) are advantageous to obtaining complete images of the inspected parts, although a technical interpretation performed by a team of experts in non-destructive testing (NDT) techniques is needed above all when the target is composed, as in our case, by different materials. On the other hand, optical coherence tomography (OCT) is slow when inspecting complete parts, but it has great level of structural detail in subsurface measurements up to 3 mm. The complementary use of these two techniques, and its application to a very ancient marquetry sample with an unusual tessellatum layer, is presented herein. The plan size of the sample is 208×212 mm, while the tessellatum is 1.5 mm thick. Starting from thermal imaging inspections, using step-heating (SH) and pulsed thermography (PT), a defect map has been defined. Structural details of these defects using OCT will help the restorer in charge of the restoration process to perform a satisfactory work.

Keywords Active infrared thermography · OCT · NDT · Restoration · Defect detection

1 Introduction

The studies of conservation to preserve the state of artworks are focused on both the degradation of materials and the links between the diverse materials that form them. Qualitative and quantitative changes in physical parameters of materials offer information on their degradation. Thermal parameters such as conductivity, specific heat and emissivity have been

shown as a powerful tool to demonstrate the degradation of materials and parts investigated [1].

Infrared thermography (IRT) has proved to be a useful technique for the study of such properties. During the last decades, it has been used in different fields and in a great variety of applications [2–4]. It presents an important series of advantages. In fact, it is non-destructive, non-contact, can be applied in situ, does not require an extremely controlled environment, it is based on non-ionizing radiations, i.e. no dangerous for people. In addition, it is based on images, called thermograms, that make it comprehensive and attractive to understand the collected data.

IRT can be passive or active. In the first one, the features of interest are naturally at a higher or lower temperature than the background. The information it offers is therefore limited since the thermal contrast is moderate. In active IRT, an energy source is required to produce a thermal contrast between the feature of interest and the background. Then, the thermograms can be processed by obtaining subsurface information from the sample, as well as quantitative evaluations of defects in it.

✉ Francisco J. Madruga
madrugaf@unican.es

1 Photonics Engineering Group, CIBER-BBN and IDIVAL, Universidad de Cantabria, Plaza de la Ciencia s/n, 39005 Santander, Cantabria, Spain

2 Department of Industrial and Information Engineering and Economics (DIIIE), University of L'Aquila, Piazzale E. Pontieri 1, Monteluco Di Roio, 67100 L'Aquila, AQ, Italy

3 Tomsk Polytechnic University, Savinykh St., 7, Tomsk, Russia634028

4 Individual Company of Restoration (Gianfranco Gargiulo), Via Tiberio 7b, 80073 Capri, NA, Italy

Although its use is widespread and successful in many cases, it offers several limitations such as an excessive heating in some cases [5].

The optical coherence tomography (OCT) technique directs a beam of light to the object to be inspected and measures the delay in the echo of the light when it is reflected from the microstructures by means of a Michaelson interferometer. This measurement provides an axial scan (A-Scan), representing a reflectivity profile that has location information and dimensions of the artefacts and/or defects within the sample. By sweeping a scanning mirror, adjacent A-scans are acquired forming a bidimensional image of reflectivity information (B-Scan). OCT's advantages complement those of active IRT by producing very little heating in the artworks. In addition, it is be able to resolve in depths of few millimetres with micrometric resolutions. However, it requires positioning the OCT probe sequentially in different areas (10 by 10 mm^2) to analyse the whole piece.

The presented NDTs show a complementary behaviour and accordingly the following section proposes a methodology based on the fusion of both techniques. The methodology improves the information offered by a professional restorer in focalised areas of the artwork defined previously by IRT and OCT.

2 Materials and Methodology

In this work, the authors propose the use of a methodology based on active IRT complemented with the OCT measurement technique for defect detection in marquetries and offer a tool to restorers providing a defect map of the complete piece. Due to the heating time necessary to inspect the marquetry, the thermograms that should provide information on the closest defects to the surface are saturated. With the OCT technique we will have data from the inspection of the so-called blind or blinded depth.

2.1 Sample Description

An original marquetry of unknown and very old origin has been used herein (Fig. 1). It has a layer of tesserae of different materials that makes it quite unusual, by increasing at the same time its historical value. From an aesthetics point-of-view, it should come from Middle East or North Africa. It is believed to belong to a parietal roof or to a proper roof. The size is $208 \times 212 \times 16$ mm.

The geometric marquetry is composed by a layer of tesserae of different size and shape. The raw material was first sawed by hand into thin sheets (there are, in the verse, small signs of work related to a handsaw) with a suitable thickness, and then cut into different small pieces.

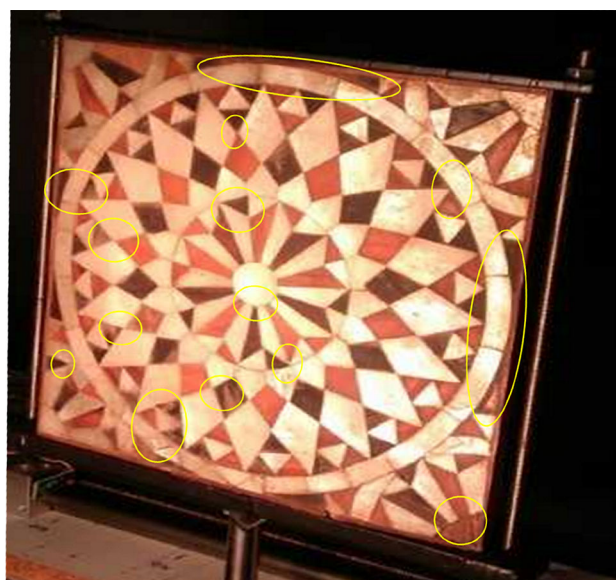Possible defects that may be found include:

Fig. 1 Tested marquetry sample and the main defect positions

- Deformation due to lift of the support.
- Small surveys caused mainly by both the deformation and the simultaneous reduction of the support.
- Some tesserae are deformed and tend to rise.
- Very small holes that have a quadrangular section.
- Internal presence of other materials between tesserae and support, rest of glue and metals (nails, etc.).
- Cracks through the support.
- Presence of rust on the tessellatum layer.

2.2 Optical Coherent Tomography (OCT)

OCT is a scanning technique allowing for the investigation of objects moderately attenuating the probing light in reflection geometry. OCT employs partly coherent, polychromatic light from the near infrared region (0.7–1.5 μm) that is analysed in an interferometer after being reflected by the sample. Interfaces between layers with different refractive index or scattering coefficient reflect the light back to the interferometer allowing for the acquisition of depth profiles (typically around or below 3 mm in depth), virtual cross of few squared millimetres sections and 3-dimensional data sets. A huge list of applications of OCT to the investigation of various cultural heritage items have been presented [6].

The experiments are performed using a Thorlabs OCS1300SS OCT system. The system has a laser light source centred at 1320 nm, with a spectral bandwidth of 100 nm and an optical output powerup to 10 mW. This power level is considered non-invasive even for light-sensitive materials and biological tissue. In practice, the ability to differentiate thin layers is defined by the axial (in-depth) resolution. The specified axial resolution is 12 μm with a penetration of
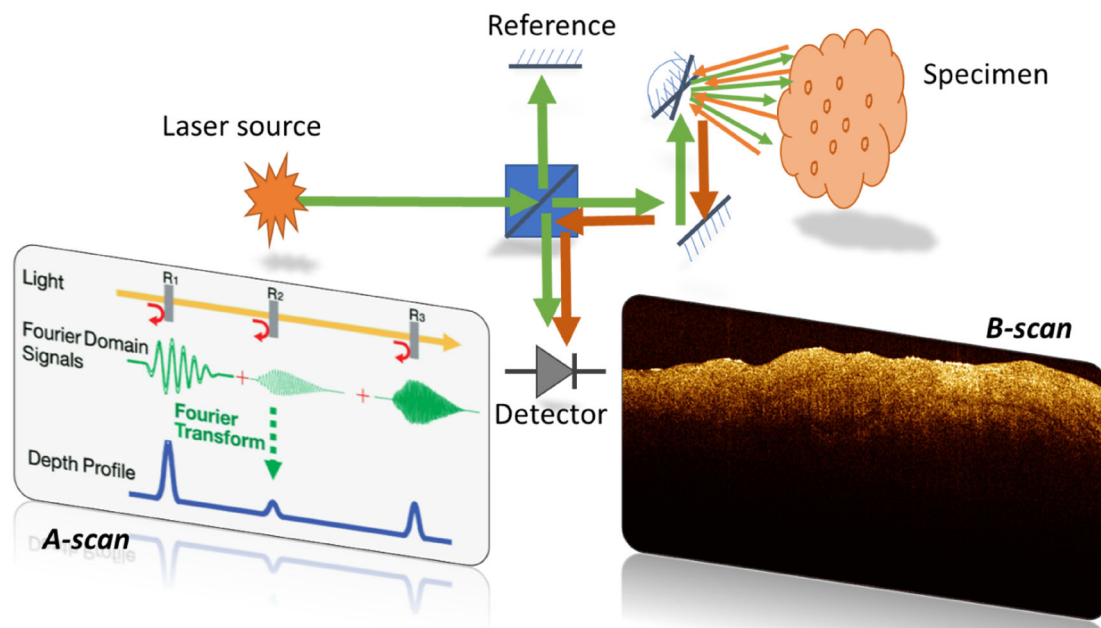
Fig. 2 Scheme of OCT system

3 mm (in air). Lateral resolution (the ability to differentiate between structures occurring close to each other in lateral plane) is 25 µm.

The distance to the examined object from the most protruding element of the device is 2.54 mm and the structural information from the area up to $10 \times 10 \, mm^2$ may be acquired in each single measurement. Data collection time for one 2D cross-section (B-scan) is below 30 s.

The advantages of OCT technique include:

- The intensity and wavelength of used light source is non-invasive, for both the sample integrity and the operator.
- To provide improved representativeness of results (one, two or three-dimensional representation), in comparison to traditional, invasive sampling methods.
- To provide structural information in depth.

The major limitation of what may be examined with OCT lies in the transparency of subsurface structures of the object to infrared radiation.

OCT results are usually presented as cross-sectional views, although some other post processing of the data enables revealing additional features of the object.

The structure of the examined object is shown in a false colour scale: warm colours correspond to high scatter/reflection of the probing light, whereas cold colours mark areas with low scatter. Transparent media at the wavelength of the system (e.g. clear varnishes, glass or air above the surface of the examined object) or areas located beyond the range of penetration are shown dark. The 'strongest' line is usually due to specular reflection at the air-target interface.

If series of adjacent scans are collected over an area, they comprise a 3-D volume of data points. We can present the data as the slice of voxels of a given thickness extracted from the data cube at a given depth, always parallel to the surface of the painting and thus independently of its tilt, or as 'slice' of the voxels extracted from data cube for a line of surface including depth data (B-Scan image). Four measurements are averaged at each voxel to reduce speckle noise. Figure 2 resumes the OCT method.

It is important to note that the distances along the probing beam are seen in OCT as optical ones. Therefore, to measure true axial distances within the structures in the object (e.g. the layers' thicknesses) one must divide a distance obtained with the scale bar by the refractive index of the material (n). The thickness of tessellatum layer has been cleaned and measured using a gauge. The axial distance of OCT equipment is 3 mm in air ($n = 1$) and the refraction index of tessellatum can be calculated using $n = 3/measured \, depth$ for each tessellatum type. Table 1 shows the results to correctly define the scale bar in B-Scan image.

Figure 3 (B-Scan of defect T1) shows an obvious defect, i.e., the lack of tessera; is it useful to explain how this technique works. The image has 512 pixels for depth, where the dimension of pixels in microns depends on the refractive index of the medium that propagates the laser wave. In air, the penetration is of 3 mm, giving a resolution of 3/512 mm/pixel. In the right area there is no tessellatum and the medium is air with refractive index equal 1. *Zreal* is a measure of exact axial distance in pixels within the image (see Fig. 3), by knowing the index of refraction throughout its trajectory that serves

Table 1 Tesserae, thicknesses and refractive indices

Alleged or suspected material	Tesserae	Thickness (mm)	Refractive Index
Mother of pearl	White tesserae	1.44	1.44
Bovine horn, probably cow	Amber/grey tesserae	1.23	1.25
Horn or tortoise	Some brown tesserae	1,28	1.22
Horn of another ungulate	Some brown/black tesserae	1.32	1.22

Table 2 Summary of optical excitations used in IRT tests

Excitation	Power (W)	Excitation time/lock-in frequency	Recorded images
Flash lamp	6600	300 ms	188
Step heating halogen lamps	1800	30 s	488
	1800	100 s	788
	1800	300 s	1088

as a reference to calculating the value of the thickness of the tessellatum in mm with the expression (1)

$$Thickness \text{ (mm)} = \frac{3}{512} \times Zreal \text{ (px)} \quad (1)$$

In the left area, tessellatum is displayed and it seems that the interface with the wood has a different depth. But no, it is an effect of the Refractive Index. It is necessary to know the refractive index of the tessellatum. Knowing, in pixels, the value of the Δz value as the difference in depth between the value measured in air with Refractive Index = 1 and the value measured through the tessellatum with unknown refractive index, we can determine the refractive index of the tessellatum, using (2).

$$n\text{(tessalum)} = \frac{512}{3} \times \frac{Thickness \text{ (mm)}}{(Zreal + \Delta z)\text{(px)}} \quad (2)$$

Figure 3 also shows the different scattering of the materials, seen as different textures between wood and tessellatum. The information detectable with this technique is due either to scattering or to reflection at the interfaces. The beginning
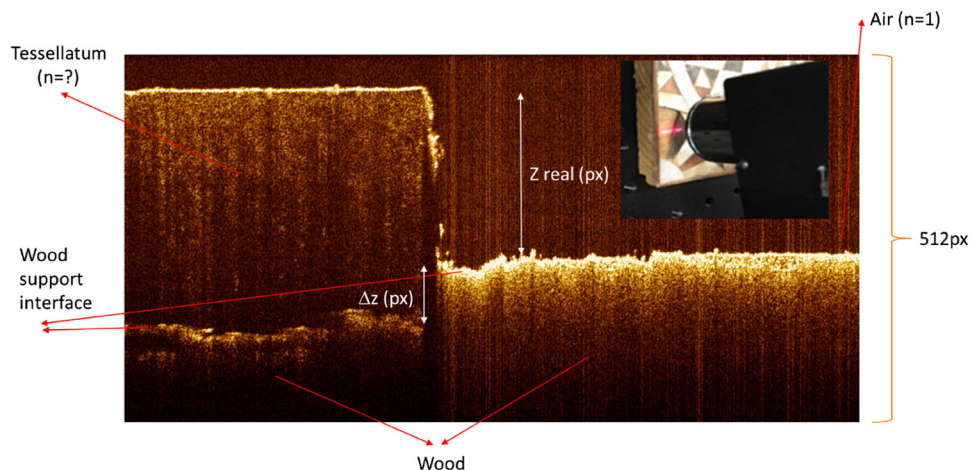
of the tessellatum and the wooden support is defined as well as the tessellatum-wood interface.

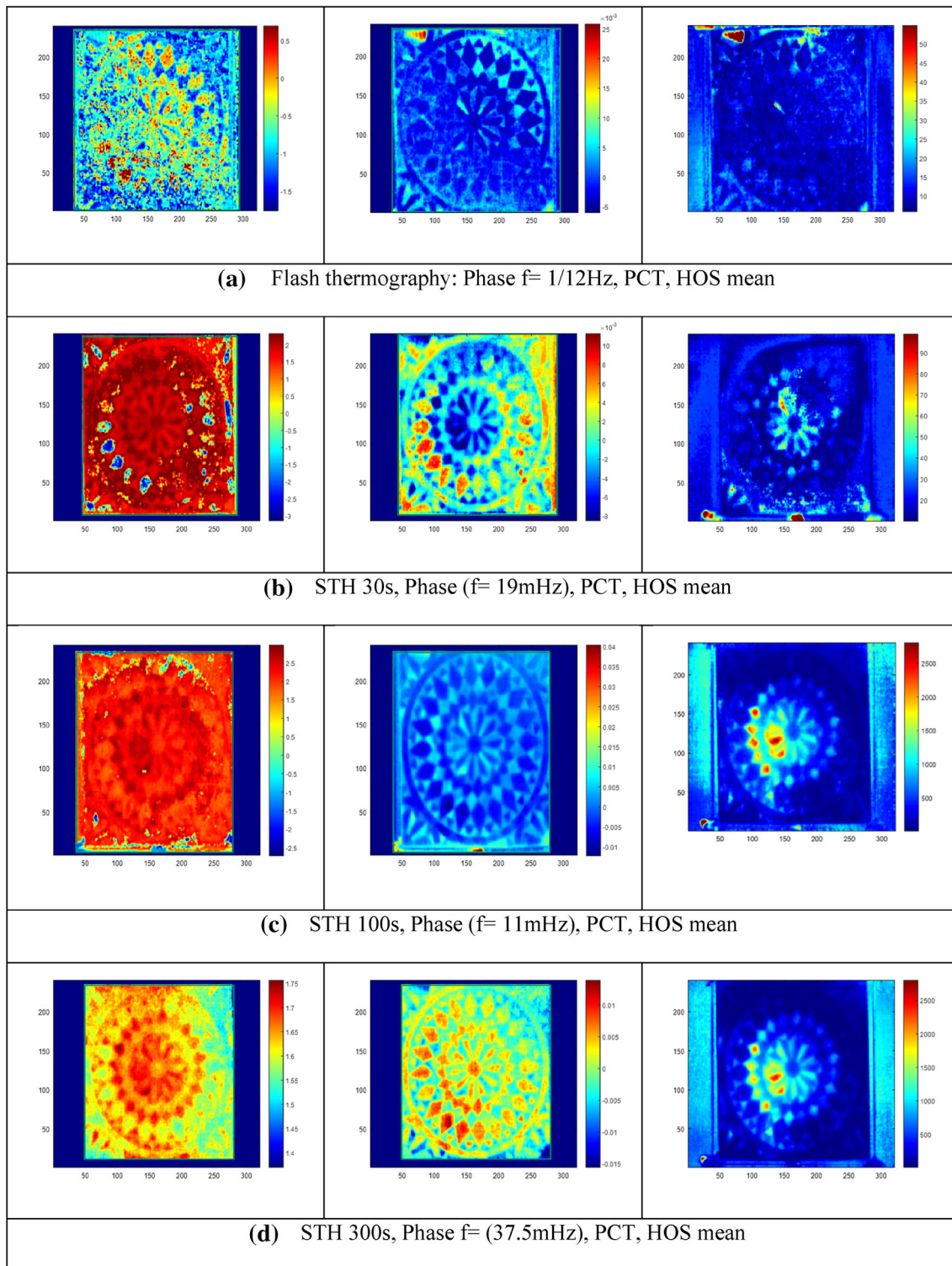## 2.3 Active Infrared Thermography (IRT)

The detection of defects using IRT technique is because defects included in the structure and the inspected structure have different thermal behaviour. When a structure has void areas or inhomogeneities, both density and thermal conductivity increase or decrease while thermal diffusivity, defined as ratio of thermal conductivity to the volumetric heat capacity, changes. This change is observable from the surface temperature changes; therefore, the defects can be marked. If the defect is subsurface, the measured surface temperature will be modified as result of the thermal inertia from the hot spot originated in the subsurface defect.

Already said before, the experiments in this work are based on a FLIR SC 2000 thermal camera and optical source excitations. The heat generated by the optical source is propagated via thermal waves from the surface onto the structure. When the heat reaches a defect, the diffusivity value changes, and the thermal inertia causes the appearance of a thermal imprint at the surface. Heat can be generated by flashes, LEDs (Light-Emitting Diodes) and halogen lamps, resulting in short pulses of thermal waves (Pulse Thermography, PT), long pulses or steps (SHT), waves in lock-in mode

Fig. 3 Details of OCT performance. OCT provides depth measurement difference depending on the refractive index of the material passing through. If the measurement is through air with known refractive index (n = 1), then depth measurement can be calculated. The depth measurement offered by OCT is increased with respect to the real one (Δz) when the medium that passes through has an n > 1

(a)   Flash thermography: Phase f= 1/12Hz, PCT, HOS mean

(b)   STH 30s, Phase (f= 19mHz), PCT, HOS mean

(c)   STH 100s, Phase (f= 11mHz), PCT, HOS mean

**(d)**   STH 300s, Phase f= (37.5mHz), PCT, HOS mean

Fig. 4 Thermography measurements: **a** Flash thermography, **b–d** step heating thermography at different stages and its processing with phase Fourier transform (PPT), principal component thermography, and High-order statistics (mean value)

(Lock-in Thermography, LT) or coded-waveforms. Pulse-compression thermography has recently been combined with coded-waveforms by obtaining very low ΔT increments in cultural heritage items [7, 8]. The thermographic tests presented here have been carried out with PT using 3300 W flashes, and six halogen lamps of 300 W each for SHT.

(a)

(b)
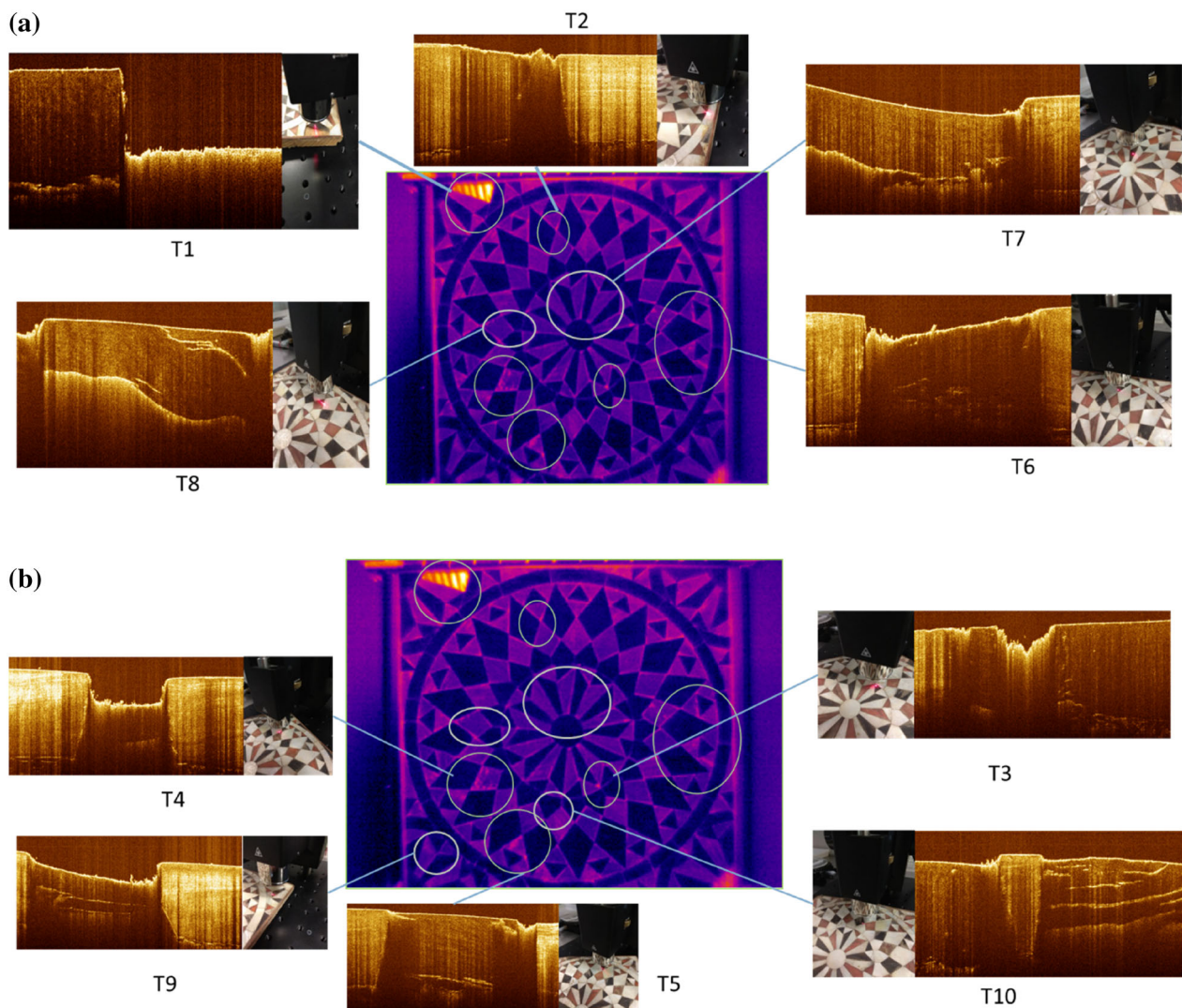
Fig. 5 **a** B-Scan and photograph of the defects T1, T2, T6, T7 and T8. A link with a thermogram is provided. **b** B-Scan and photograph of the defects T3, T4, T5, T9 and T10. A link with a thermogram is provided

Several processing techniques have been applied to highlight the defects from the raw thermography sequences, such as higher-order statistics (HOS) [9], pulsed phase thermography (PPT) [10], and principal component thermography (PCT) [11].

3 Results and Discussion

Due to the variety of materials on the surface and the lack of knowledge of the internal structure to obtain a map of defects by IRT, two thermographic excitation methods summarized in Table 2 were applied. The camera worked with a framerate of nine frames/s and to correct the background effect twelve cold thermograms have been recorded at the initial stage.

The results obtained from the processes of the four thermographic tests performed are shown in Fig. 4. The first processing performed is based on the Discrete Fourier Transform (DFT), to change from time to frequency domain. Concerning the sequences of images obtained (amplitude or phase), those of phase or *phasegrams* have a special interest because they are less affected by the effects of signal degradation. Within them, there is a frequency where the contrast of the image is greater and whose frequency value depends on the capture parameters. The information provided by this process are not very clear, while they are clearly defined for step excitations where there is a significant variation in the tesserae at the bottom left-hand corner.

The principal component analysis (PCA) transforms data into another representation where a new set of basis vectors (variables) are used [12]. In PCA, however, these basis

Table 3 Defects studied by OCT and the correlation with the thermographic data

Defect ID	OCT tomogram conclusions	Thermal data vs OCT tomogram
T1	Tessellatum disappear, different attenuation and different depth	Different surface material detected by pulse thermography. Step heating method hides the defect because of the thermal inertia when the time of excitation increases
T2	Three different materials, three different scattering. Some internal reflections appear at different depth for the same point. We find glue or other materials between tessellatum and wood	Only abnormal thermal behaviour is observed with 30-s step heating excitation and processing with HOS. This shows us only the presence of a different material between two others. The thermal sequence does not offer information on the material interposed between tessellatum and wood
T3	Surface defects	Hot spot in PCT-Pulse thermography
T4	Three different materials, three different scattering. Some internal reflections appear at different depth for the same point	Only an abnormal thermal behaviour is observed with 30-s step heating excitation and processing with HOS. This shows us the presence of a different material between two others. The thermal sequence does not offer information on the material interposed between tessellatum and wood
T5	Several interfaces in the same point and several materials due to several scattering in the sample	Hot area with 30-s and 100 s step heating excitation and processing with HOS. The thermal test detects the different materials but no internal interfaces
T6	Internal crack and irregular surface	No thermal differences
T7	The depth of the interface varies, which indicates an unknown element with the same optical properties between tile and wood	Flaw detection when pulse thermography is used
T8	Several interfaces in the same point and several materials due to several scattering in the sample	Hot area with 30, 100 and 300 s step heating excitation. Thermal conductivity is modified by the interfaces
T9	Two different materials, three different scattering. Some leak internal reflections appear at different depth for the same point	Only an abnormal thermal behaviour is observed with 30-s step heating excitation and processing with HOS. This shows us the presence of a different material between two others. The thermal sequence does not offer information on the material interposed between tessellatum and wood
T10	A lot of interfaces at the same point. This means internal cracks inside material	Only abnormal thermal behaviour is observed with 30-s step heating excitation and processing with HOS. For other higher excitation times the defect is in the blind area of measure. Lock-in thermography can be useful

vectors are not constant as is the case in many other transformations. Instead, they are calculated based on the data to be transformed. The objective is to enhance the variance of the data set. PCA is a linear transformation with orthogonal basis vectors, so it can be expressed as translation and rotation by (3):

$$y = A \cdot (x - \mu_x) \tag{3}$$

where A contains the new basis vectors, e_i is a row vectors, hence $A = [e_1\ e_2\ ...\ e_n]T$, and μ_x is the mean of the data set.

The transformed data where the ith sample is denoted $y_i = [y_{1i} y_{2i}]T$ and calculated using Eq. (3). The reader can observe that the main part of the data variance is represented in the first variable, y1. Therefore, if the second variable is ignored, the main variance of data is kept. In many cases, variance equals information, hence a more compact representation of data/information is obtained. PCT is called to second value of PCA, because the first variable contains the effect of the employed excitation as main source of variance in the data set. Two zones show certain variations in the values, i.e., the

bottom left-hand corner and the right area from the central zone.

Finally, RX, Skewness and Kurtosis are respectively the second, third and fourth standardized statistic moments of a data set also called higher-order statistics. RX is a measure of variance of the Gaussian probability distribution. Skewness is a measure of the asymmetry of the probability distribution of a real-valued random variable [13]. Finally, Kurtosis is defined as a measure reflecting the degree to which a distribution is peaked, and it provides information regarding the height of the distribution relative to the value of its standard deviation [14]. The set of these three values highlights the presence of anomalies of small size with respect to the sample size. In Fig. 4—third column, the average value of the three values that reduce false positives is shown and in turn enhances the defects that typically in IRT affect the three statistical parameters.

From the map of defects obtained using IRT, ten faulty points have been chosen to be inspected with OCT. In Fig. 5a and b, these ten points are presented with the image B-Scan measured and with a real photograph to understand the part of the inspected piece. A thermogram links the optical and visual part. The B-Scans have been called T1–T10 and in each of them, it is possible to observe a type of defect or useful information. Table 3 compares the information coming from OCT and IRT techniques to explain the thermal behaviour. The scattering and internal reflections data detected by the B-scan images allow explaining the observed thermal behaviours.

3.1 Conclusions

The complementarity of IRT and OCT techniques has been demonstrated herein in a qualitative study. Active IRT provides an overview of the marquetry sample, that was improved using three excitation techniques. By using IRT along with different algorithms it is possible to get a global map of defective areas from a comparison of the results obtained in each image [15]. Ten possible faulty areas defined with IRT have been measured thanks to OCT technique by obtaining new results useful to recognize materials or previous restorations. OCT has a depth measurement limited to less than 3 mm, which perfectly complements the blind area of pulsed IRT and step heating IRT. In addition, it helps to explaining the thermal behaviour observed.

References

1. Riccardi, A., et al.: Parchment ageing study: new methods based on thermal transport and shrinkage analysis. E-Preserv. Sci. **7**, 87 (2010)
2. Laureti, S., et al.: The use of pulse-compression thermography for detecting defects in paintings. NDT E Int. **98**, 147–154 (2018). https://doi.org/10.1016/j.ndteint.2018.05.003
3. Duan, Y., et al.: Reliability assessment of pulsed thermography and ultrasonic testing for impact damage of CFRP panels. NDT E Int. **102**, 77–83 (2019). https://doi.org/10.1016/j.ndteint.2018.11.010
4. Sfarra, S., et al.: Improving the detection of thermal bridges in buildings via on-site infrared thermography: the potentialities of innovative mathematical tools. Energy Build. **182**, 159–171 (2019). https://doi.org/10.1016/j.enbuild.2018.10.017
5. Gonzalez Fernández, D.A.: "Contribuciones a las técnicas no destructivas para evaluación y prueba de procesos y materiales basadas en radiaciones infrarrojas", PhD thesis, Universidad de Cantabria, Santander. https://www.tesisenred.net/handle/10803/10706 (2006). Accessed 11 May 2020
6. Complete list of papers on application of OCT to examination of artwork may be found at https://www.oct4art.eu: Optical coherence tomography for examination of works of art. Accessed 15 Aug 2019
7. Laureti, S., et al.: Development of integrated innovative techniques for paintings examination: the case studies of the resurrection of Christ attributed to Andrea Mantegna and the crucifixion of Viterbo attributed to Michelangelo's workshop. J. Cult. Herit. **40**, 1–16 (2019). https://doi.org/10.1016/j.culher.2019.05.005
8. Laureti, S., et al.: Looking through paintings by combining hyperspectral imaging and pulse-compression thermography. Sensors **19**(19), 4335 (2019). https://doi.org/10.3390/s19194335
9. Madruga, F.J., et al.: Infrared thermography processing based on higher order statistics. NDT E Int. **43**(8), 661–666 (2010). https://doi.org/10.1016/j.ndteint.2010.07.002
10. Ibarra Castanedo, C. Quantitative subsurface defect evaluation by pulsed phase thermography: depth retrieval with the phase. PhD thesis, University of Laval, Québec. https://corpus.ulaval.ca/jspui/bitstream/20.500.11794/18116/1/23016.pdf (2005)
11. Rajic, N.: Principal component thermography for flaw contrast enhancement and flaw depth characterisation in composite structures. Compos. Struct. **58**(4), 521–528 (2002). https://doi.org/10.1016/S0263-8223(02)00161-7
12. Moeslund, T.: Principal component analysis-an introduction. Technical Report CVMT 01–02, ISSN 0906-6233, (2001)
13. Madruga, F., et al.: Automatic data processing based on the skewness statistic parameter for subsurface defect detection by active infrared thermography. In: Proceedings of QIRT 9–Quantitative Infrared Thermography (2008)
14. Madruga, F.J., et al.: Enhanced contrast detection of subsurface defects by pulsed infrared thermography based on the fourth order statistic moment, kurtosis. In: Proceedings on SPIE 7299, Thermosense XXXI. https://doi.org/10.1117/12.818684
15. Sfarra, S., et al.: Qualitative assessments via infrared vision of subsurface defects present beneath decorative surface coatings. Int. J. Thermophys. **39**, 13 (2018). https://doi.org/10.1007/s10765-017-2333-4